

# Topological insulators in dynamically generated lattices

O. Dutta<sup>1,2\*</sup> and A. Przysiężna<sup>3,4</sup>, and M. Lewenstein<sup>1,5</sup>

<sup>1</sup> ICFO–Institut de Ciències Fotòniques, Av. Carl Friedrich Gauss, num. 3, 08860 Castelldefels (Barcelona), Spain

<sup>2</sup> Instytut Fizyki imienia Mariana Smoluchowskiego, Uniwersytet Jagielloński, ulica Reymonta 4, PL-30-059 Kraków, Poland

<sup>3</sup> Institute of Theoretical Physics and Astrophysics, University of Gdańsk, Wita Stwosza 57, 80-952 Gdańsk, Poland

<sup>4</sup> National Quantum Information Centre of Gdańsk, Andersa 27, 81-824 Sopot, Poland

<sup>5</sup> ICREA – Institució Catalana de Recerca i Estudis Avançats, Lluís Companys 23, E-08010 Barcelona, Spain

(Dated: March 11, 2019)

Topological insulators are of fundamental and technological importance due to their exotic excitations that allow for robust transport of charges (matter) on the boundary and thus have potential applications in spintronics, quantum computing [1] and spintomics [2]. In this regard, due to the enormous control and possibility of quantum engineering, systems of ultracold gases trapped in optical lattices open promising avenues to follow. In this paper we show that starting from a trivial lattice, one can dynamically generate topologically non-trivial lattice which can host topologically insulating states in the form of Quantum Anomalous Hall states or Quantum Spin Hall states. We investigate the necessary experimental conditions to generate such states.

PACS numbers: 67.85.Lm, 03.75.Lm, 73.43.-f

Currently, there is great interest in investigating solid-state systems supporting topologically insulating states [3–5]. In the field of ultracold quantum gases, such systems can be achieved by optical creation of frustrated lattice geometries, as well as by generating tunable long-range hopping amplitudes [6–15]. Recently, other ways to induce topologically insulating states such as Quantum Anomalous Hall states (*QAH*) and Quantum Spin Hall states (*QSH*) were investigated. Particularly interesting is the creation of interaction-driven topological insulators in lattices with quadratic band-crossing points (*QBCP*) [16, 17]. In these proposals the long-range tunneling responsible for *QAH*/*QSH* states originates from the mean-field effect of the interaction. In this letter we propose to create such non-trivial lattice structure (in particular a Lieb lattice) dynamically due to interaction induced self-organization of an ultracold gas. Moreover, one also dynamically generates pseudo-spin degrees of freedom. Consequently, we show that in our system one can study the appearance of interaction-driven *QAH* and/or *QSH* states. Our findings also sheds light on a novel way to look into a physical system where particles live in interaction-induced emergent structures with exotic dispersion relations.

## Model

We consider a mixture of two species ultracold fermionic atoms trapped in an optical lattice potential  $V_{\sigma,\text{latt}} = V_{\sigma,x} \sin^2(\pi x/a) + V_{\sigma,y} \sin^2(\pi y/a) + V_{\sigma,z} \sin^2(\pi z/a)$ , where  $\sigma = \uparrow, \downarrow$  denotes the two species and  $V_{\sigma,x(y)(z)}$  are the corresponding lattice depths for  $\sigma$ -fermions along the  $x, y, z$  direction respectively. For the two-dimensional (*2D*) geometry we choose  $V_0 = V_{\downarrow,x} = V_{\downarrow,y}$ ,  $V_1 = V_{\downarrow,z} = V_{\uparrow,x(y)(z)}$ , and  $V_1 \gg V_0$ , so that the  $\downarrow$ -fermions can effectively move in the  $x - y$  plane with the

$z$  motion freezed. As the  $\uparrow$ -fermions move in a deeper lattice, we can neglect the tunneling of this particles. For simplicity we consider the case in which fermionic masses are equal  $m_{\downarrow} = m_{\uparrow}$ , which implies equal recoil energies  $E_R = E_{R\sigma} = \pi^2 \hbar^2 / 2m_{\sigma} a^2$ . In this paper we look into spin-imbalanced situation with filling  $n_{\downarrow} = 1$  and  $n_{\uparrow} = 1/2$ . Atoms of different types interact with each other via the  $s$ -wave scattering with strength  $a_s$ . If the interaction is strongly attractive ( $a_s \ll 0$ ), the  $\uparrow$  and  $\downarrow$ -fermions tend to pair and form composites with creation operator  $\hat{b}_i^{\dagger} = \hat{s}_{i\uparrow}^{\dagger} \hat{s}_{i\downarrow}^{\dagger}$  and corresponding number operator  $\hat{n}_i^B$  [18–20]. Here  $\hat{s}_{\sigma i}^{\dagger}, \hat{s}_{\sigma i}$  are the creation and annihilation operators of the  $\sigma$  fermions in the respective  $s$ -bands. The composite density is the same as the  $\uparrow$ -fermions density, i.e. in our case  $n_{\uparrow} = n^B = 1/2$ . Such pairs can tunnel only due to the second order processes which are practically negligible. The excess  $\downarrow$ -fermions with the filling  $m = n_{\downarrow} - n_{\uparrow} = 1/2$ , and can tunnel from one site to another. Recently it has been noted that in the strong interaction regime, the standard Hubbard models have to be modified due to both intra- and inter-band effects [21–23]. Taking these effects into account we construct a minimal model for the composites and the excess  $\downarrow$ -fermions by including the occupation of the  $s$  and  $p$ -bands and the renormalization of the interactions.

## Modified Hamiltonian

The inclusion of  $p$ -bands allows one  $\downarrow$ -fermion to occupy the same site as a composite. The single-particle tunneling Hamiltonian then reads:

$$H_t = -J_0 \sum_{\langle ij \rangle} \hat{s}_i^{\dagger} \hat{s}_j + J_1 \sum_{\delta} \sum_{\langle ij \rangle_{\delta}} \hat{p}_{\delta i}^{\dagger} \hat{p}_{\delta j}, \quad (1)$$

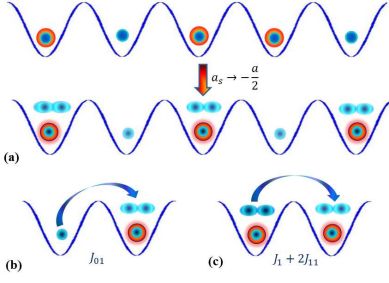


FIG. 1. A one-dimensional schematic representation of the system considered in the paper. A red larger sphere refers to a  $\uparrow$ -fermion and a smaller blue sphere represents a  $\downarrow$ -fermion. (a) Top figure: One creates a band insulator for the  $\downarrow$ -fermions and half-filled system for the  $\uparrow$ -fermions in presence of weak interactions. Bottom figure: Increasing the attractive scattering length  $a_s$  leads to an emergence of composites that form a checkerboard structure and the remaining  $\downarrow$ -fermions move between  $s$ - and  $p$ -orbitals (semi-transparent blue spheres and dumbbells). (b) The interaction induced  $s-p$  band hybridization tunneling element corresponding to Hamiltonian (3). (c) The effective tunneling in the  $p$ -band when two composites occupy neighbouring sites.

where  $\delta = x, y$  and  $\hat{s}_i^\dagger, \hat{s}_i, \hat{p}_\delta^\dagger, \hat{p}_\delta$  are the creation and annihilation operators of the  $\downarrow$  particles in the  $s$ - and  $p$ -bands respectively.  $J_0, J_1 > 0$  are the single-particle tunneling amplitudes in the  $s$ - and  $p$ -band respectively, and  $\langle \mathbf{ij} \rangle_{x(y)}$  denotes the nearest-neighbour sites along the  $x(y)$ -direction. The on-site Hamiltonian for the excess  $\downarrow$ -fermions and the composites including the  $s$ - and  $p$ -bands is given by:

$$H_{\text{int}} = -|U_2| \sum_{\mathbf{i}} \hat{n}_{\mathbf{i}}^B - |U_3| \sum_{\mathbf{i}} \hat{n}_{\mathbf{i}}^B (\hat{n}_{x\mathbf{i}} + \hat{n}_{y\mathbf{i}}) - |\delta U_3| \sum_{\mathbf{i}} \hat{n}_{x\mathbf{i}} \hat{n}_{y\mathbf{i}} \hat{n}_{\mathbf{i}}^B + E_1 \sum_{\mathbf{i}} (\hat{n}_{x\mathbf{i}} + \hat{n}_{y\mathbf{i}}), \quad (2)$$

where  $\hat{n}_{x(y)\mathbf{i}} = \hat{p}_{x(y)\mathbf{i}}^\dagger \hat{p}_{x(y)\mathbf{i}}$ . The renormalized self-energy of the composite is given by  $U_2$  whereas  $U_3$  is the strength of the renormalized onsite interactions between a composite and a  $\downarrow$ -fermion in the  $p$  band at a given site.  $\delta U_3$  denotes the effective three-body interaction between one composite and two  $\downarrow$ -fermion each in the  $p_x$  and  $p_y$  orbitals. One should note that such higher-body interactions like  $\delta U_3$  are already probed in ultracold atom experiments [25]. We find that  $\delta U_3$  is small compared to other parameters, so we neglect it at first. Then the energy cost for a excess  $\downarrow$ -fermions to sit in the  $p$ -band of a composite occupied site is given by

$$\Delta = E_1 - |U_3| + |U_2|,$$

and can be reduced as one increases the attractive scattering length. Then, the  $\downarrow$ -fermions can only occupy the  $p$ -orbital of a site with a composite, when  $\Delta$  is small or negative.

Next we consider the modifications originating from the nearest-neighbour scattering due to the interaction between the excess  $\downarrow$ -fermions and the composites. One of them mixes the  $s$ - and  $p$ -bands and can be written as

$$H_{01} = J_{01} \sum_{\delta=x,y} \sum_{\langle \mathbf{ij} \rangle_\delta} \zeta_{i_\delta, j_\delta} \hat{p}_{\delta\mathbf{i}}^\dagger \hat{n}_{\mathbf{i}}^B \hat{s}_{\mathbf{j}} + h.c., \quad (3)$$

where  $J_{01}$  denotes the interaction induced inter-band tunneling and  $\zeta_{i_\delta, j_\delta} = (-1)^{i_\delta - j_\delta}$  reflects the staggered nature of the  $s-p$  tunneling matrix. This process is shown pictorially in Fig.1(c). Such natural non-local hybridization between  $s-p$  bands due to interaction induced tunneling is an important feature of the strongly interacting gases in lattices; it is worth to stress that such processes are usually neglected in the literature. Next, we write the interaction-induced tunneling in the  $p$ -band as:

$$H_T = J_{11} \sum_{\delta} \sum_{\langle \mathbf{ij} \rangle_\delta} \hat{p}_{\delta\mathbf{i}}^\dagger (\hat{n}_{\mathbf{i}}^B + \hat{n}_{\mathbf{j}}^B) \hat{p}_{\delta\mathbf{j}}, \quad (4)$$

where  $\delta, \delta' = x, y$  with  $\delta \neq \delta'$  and  $J_{11}$  denotes intra-band interaction-induced tunneling for  $p_x(p_y)$ -fermions along  $x(y)$  directions.  $H_T$  gives the most important contribution to the renormalization of intra-band tunneling [24]. Thus from Fig.1(c) we see that tunneling in  $p$ -band is only possible when two neighbouring sites are occupied by composites as this process conserves energy. As for  $a_s < 0$ , the interaction-induced tunneling  $J_{11}$  is negative, the effective tunneling in the  $p$ -band (given by  $J_1 + 2J_{11}$ ) decreases with increasing attraction. Thus in the region where  $|J_{01}| \approx |J_1 + 2J_{11}|$ , the excess  $\downarrow$ -fermions prefer a configuration like Fig.1(b) with alternating sites occupied by composites. The relevant tunneling parameters are only controlled by the effective interaction  $\alpha = a_s/a$  and the lattice depths. The derivations of the various tunneling and interaction parameters using Wannier functions are discussed in the *Supplementary material*.

### Dynamical Lieb lattice

The total Hamiltonian  $H = H_t + H_T + H_{01} + H_{\text{int}}$  does not contain any tunneling of the composites, which makes the commutator  $[\hat{n}_{\mathbf{i}}^B, H] = 0$ . In such case  $n_{\mathbf{i}}^B = 0, 1$  becomes a good quantum number for the system. The ground state of the Hamiltonian  $H$  can be found by comparing the energies for different configurations of  $n_{\mathbf{i}}^B$  over the entire lattice by solving the corresponding single particle Hamiltonian  $H$ . We have found the lowest energy configurations of the composites for various parameters by using simulated annealing method on a  $8 \times 8$  lattice with periodic boundary conditions. The phase diagram Fig.2(a) shows obtained dependence of the configuration of composites on the parameters  $\alpha$  and  $V_1$ . We distinguish the following phases: i) checkerboard

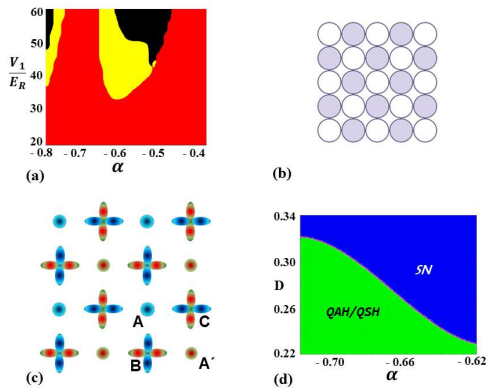


FIG. 2. (a) We plot the phase diagram for the configurations of the composites. The red coloured region denotes the period-1 checkerboard configuration for the composites. The black region denotes the phase-separated phase, the yellow region contains mixed phase. The shallow lattice parameter is  $V_0 = 4E_R$ . (b) Distribution of the composites in the *CH1* phase. The filled (empty) circles denotes presence(absence) of a composite. (c) Orbital degrees of freedom for the excess  $\downarrow$ -fermions in *CH1* lattice. The coloured circle denotes the *s*-orbitals. The horizontal (vertical) coloured dumb-bell shapes denotes  $p_x$  ( $p_y$ )-orbitals. We also show the basis states for the blue (red) lattice **A**, **B** and **C** (**A'**, **B'** and **C'**). (d) The ground state phase diagram corresponding to the Hamiltonian (6) as a function of dipolar strength  $D$  and contact interaction strength  $\alpha$  for  $V_0 = 4E_R$ . The blue region denotes spin-nematic (SN) phase whereas the green region denotes QAH/QSH phases.

structure with period one (*CH1*-the red region, shown in Fig.2b), ii) mixed phase characterized by absence of any periodic structure (the yellow region) and iii) the phase-separated state (black) characterized by the clustering of the composites to one region of the lattice. One should

keep in mind that the total Hamiltonian  $H$  has similar features to the celebrated Falicov-Kimball (FK) model, where one can get a zoo of discontinuous structural phase transitions for different filling fractions [26]. However, in present model, the important distinction is that the standard FK models do not possess the correlated multi-orbital tunneling processes as described in this paper. The mixed phase occurs in the region where the energy cost to occupy the  $p$ -orbital is small compared to other tunneling processes. Thus it is possible that the mixed phases contain self-generated disorder due to the composite density dependence on the tunneling processes. We have checked the existence of the mixed phases and obtained phase-boundaries also for lattice sizes of  $12 \times 12$  and  $16 \times 16$  and the phase boundaries remain qualitatively unchanged. The *CH1* region is the most interesting one with respect to generation of non-trivial topological lattices. The presence of *CH1* region can be qualitatively predicted for  $\Delta \ll 0$ . It can be easily showed that the *CH1* structure has the lowest energy provided  $2J_{01}^2/|\Delta| > |J_1 + 2J_{11}|/\pi$ . Due to the directional nature of the inter-orbital tunneling  $J_{01}$  in the Hamiltonian (3) and the absence of any on-site orbital mixing term in (2), the motion of the excess fermions can be divided into two sub-lattices shown by blue and red colour in Fig.2(c). Each of the red and blue sub-lattices has the structure of an exotic Lieb lattice. In Fig.2(c) we also show the basis sites for the blue Lieb lattices denoted by **A**, **B** and **C** (**A'**, **B'** and **C'** for the red Lieb lattice). We denote the excess  $\downarrow$ -fermions moving in the blue sub-lattice by  $\Phi_1 = [\hat{s}_A, \hat{p}_{yB}, \hat{p}_{xC}]$  and the corresponding operators in the red sub-lattice by  $\Phi_2 = [\hat{s}_{A'}, \hat{p}_{xB}, \hat{p}_{yC}]$ . Thus, due to the interaction one also dynamically induces pseudo-spin degrees of freedom in form of orbitals in different sub-lattices. Their motion is governed by the Hamiltonian,

$$\begin{aligned}
 H = J_{01} & \left[ \sum_{\langle ij \rangle_x} \zeta_{i_x, j_x} \hat{s}_{Ai}^\dagger \hat{p}_{xCj} + \sum_{\langle ij \rangle_y} \zeta_{i_y, j_y} \hat{s}_{Ai}^\dagger \hat{p}_{yBj} + \sum_{\langle ij \rangle_x} \zeta_{i_x, j_x} \hat{s}_{A'i}^\dagger \hat{p}_{xBj} + \sum_{\langle ij \rangle_y} \zeta_{i_y, j_y} \hat{s}_{A'i}^\dagger \hat{p}_{yCj} + h.c \right] \\
 & + \Delta \sum_{i, \tau=B, C} (\hat{n}_{\tau xi} + \hat{n}_{\tau yi}) - |\delta U_3| \sum_{i, \tau=B, C} \hat{n}_{x\tau i} \hat{n}_{y\tau i}.
 \end{aligned} \tag{5}$$

Here the first term (the one inside the  $[\cdot]$ -bracket) in Eq.(5) is a reformulation of  $H_{01}$  in Eq(3). The second term refers to the energy cost of the  $p$ -orbital atoms occupying a site already taken by a composite. The third term describes effective onsite interactions between the red and blue fermions in the sites  $B$  and  $C$ . The single particle dispersion relation of a Lieb lattice is given by

$$\epsilon_{\mathbf{k}} \in \{ \Delta, \Delta/2 \pm \sqrt{(\Delta/2)^2 + 4J_{01}^2 [\sin^2 k_x a + \sin^2 k_y a]} \},$$

where momentum  $\mathbf{k} = (k_x a, k_y a)$  belongs to the reduced Brillouin zone  $(-\pi/2, \pi/2)$ . The dispersion contains a QBCP for  $\Delta \neq 0$  with one of the dispersive bands touching the flat band at momentum  $(0, 0)$ . For  $\Delta = 0$ , three bands touch each other at the momentum  $(0, 0)$  with the upper and lower band having linear dispersion in the vicinity of this point. For simplicity let us consider only the case when  $\Delta < 0$ . We can write an effective two band Hamiltonian  $H = d_0 \mathcal{I} + d_z \sigma_z + d_x \sigma_x$ , where

$\sigma_{x(z)}$  are the Pauli matrices,  $\mathcal{I}$  is the identity matrix,  $d_0 = (J_{01}^2/\Delta)(\cos 2k_x a + \cos 2k_y a)$  and the vector  $\vec{d} = (d_x, d_z) = (J_{01}^2/\Delta)(\cos 2k_x a - \cos 2k_y a, 4 \sin k_x a \sin k_y a)$ . In this limit, the particles occupy only the  $B$  and  $C$  sites of the lattice and the population in the  $A$  and  $A'$  sites is negligible. For excess fermion filling  $m = 1/2$ , the dispersive band is filled and the system becomes a band insulator. The vector  $\vec{d}$  acts like an effective magnetic field and the corresponding Berry phase is given by  $2\pi$ . This makes the QBCP topologically stable. Moreover, as the upper band in QBCP is flat, any fluctuations to this band can not provide conduction of the fermions. In this regard, this phase is akin to a topological band-insulator.

We would like to point out that even if generation of  $CH1$  structures have been studied in depth in the literature with respect to different long-ranged models, or mixtures [27], but possibility of the emergent lattice structures was not realized. Summarizing, in this section we have showed that, due to interaction-induced tunneling, one can dynamically generate topologically protected exotic lattices from simple geometry.

### Proposed experimental realization

For experimental realization, one should start with a band insulator for the  $\downarrow$ -fermions and half-filling for the  $\uparrow$ -fermions trapped in a square lattice where the interspecies interaction is weak. Then by adiabatically increasing the scattering length in the attractive regime via Feshbach resonance one can reach the regime of dynamical Lieb lattice. As one gets to the region with  $\Delta \approx 0$ , dynamical Lieb lattice is created due to the checkerboard structure of the composites. The experimental signature of such lattice can be detected by time-of-flight experiments where the  $\uparrow$ -fermions will show four peaks corresponding to the structure factor of the checkerboard lattice, whereas the  $\downarrow$ -fermions will show additional peaks corresponding to the orbital nature of the dynamical fermions in the Lieb lattice. Due to the appearance of the  $CH1$  over a wide range of lattice depths and scattering lengths, as shown in Fig.2a, it is indicative that this result is stable under small changes of parameters. Regarding the relevant atomic species for such experiments, one such choice could be Fermionic  ${}^6\text{Li}$  species in the two lowest energy states with broad Feshbach resonance for the interaction strength  $\alpha = a_s/a = -0.6$ . For a lattice constant of  $a = 500\text{nm}$ , the corresponding scattering length is in the order of  $a_s \sim -300\text{nm}$ . This is already achieved in Lithium mixtures in Refs. [28, 29]. The other option is a mass-imbalanced mixture. In such case the effective scattering length is scaled and  $\alpha \approx (a_s/a)(1 + m_\downarrow/2m_\uparrow)$  for the same parameters as used in the case of equal mass. Thus, if one traps  ${}^{40}\text{K}$  in the weaker lattice of  $V_0 = 4E_{R\downarrow}$  ( $\downarrow$ -fermions) and  ${}^6\text{Li}$  in the stiffer lattice of  $V_1 = 30E_{R\uparrow}$ , then the topologically protected phase for a scattering

length of  $a_s$  (KLi)  $\approx -80\text{nm}$  can be achieved. Such a strongly attractive scattering length can be experimentally realized using the narrow Feshbach resonance for  ${}^{40}\text{K}$ - ${}^6\text{Li}$  mixture by tuning the magnetic field at the milli-Gauss accuracy [30].

### Dynamical topological insulators

The dynamical realization of a Lieb lattice opens up an alternative way to study the possibility of generating integer quantum Hall effects with cold atom systems. One possible way to generate such states is by inducing effective spin-orbit coupling, which can be achieved by optical means [31], or by lattice-shaking [32]. Such coupling can also be achieved dynamically by including long-range interactions, which can create  $QAH$  and  $QSH$  states [16, 17]. Such models are usually hard to implement in experimentally realizable system, as one needs the on-site interactions to be of the same order of magnitude as the long-range part of the interaction [33]. To investigate such possibility in our system we add an extra magnetic dipolar term (restricting its range to next-nearest neighbour) for the excess  $\downarrow$ -fermions,

$$\begin{aligned}
 H_{\text{full}} &= H + H_{\text{dd}}, \\
 H_{\text{dd}} &= U_{\text{dd}} \sum_{\mathbf{i}, \tau} \hat{n}_{x\tau\mathbf{i}} \hat{n}_{y\tau\mathbf{i}} + \frac{U_{\text{xy}}}{2} \sum_{\langle\langle \mathbf{i}, \mathbf{j} \rangle\rangle, \tau \neq \tau'} \hat{n}_{x\tau\mathbf{i}} \hat{n}_{y\tau'\mathbf{j}} \\
 &\quad + \frac{U_{\text{xx}}}{2} \sum_{\langle\langle \mathbf{i}, \mathbf{j} \rangle\rangle, \tau} [\hat{n}_{x\tau\mathbf{i}} \hat{n}_{x\tau\mathbf{j}} + \hat{n}_{y\tau\mathbf{i}} \hat{n}_{y\tau\mathbf{j}}], \quad (6)
 \end{aligned}$$

where  $U_{\text{dd}}$  is an onsite dipolar interaction,  $U_{\text{xy}}$  is an interaction between the particles in  $p_x$  and  $p_y$ -orbital in  $B$  and  $C$  sites respectively, and  $U_{\text{xx}}$  is a next-nearest neighbour interaction between the particles in  $p_x$  and  $p_x$ -orbital (also between  $p_y$  and  $p_y$  orbital) in  $B$  and  $C$  sites.  $\langle\langle \mathbf{i}, \mathbf{j} \rangle\rangle$  denotes next-nearest neighbour  $p$ -orbital sites. We additionally introduce the dimensionless dipolar interaction strength  $D = \mu_0 \mu^2 m_\downarrow / 2\hbar^2 a$ , where  $\mu$  is the magnetic dipole moment of the atoms and  $\mu_0$  is the vacuum permeability. The dipole-dipole interaction has the form  $U_{\text{dd}}(r) = D(1 - 3z^2/r^2)/r^3$ , where  $r$  is the inter-particle distance. For experimental realization, the suitable candidates are: fermionic  ${}^{161}\text{Dy}$ , which is experimentally available in quantum degenerate state [34], and fermionic  ${}^{167}\text{Er}$  [35]. One can also in principle use polar molecules provided that the short range interaction could be modified, for instance, using confinement-induced resonances. Due to the strong attractive contact interaction  $|U|$ , the effect of dipolar terms on  $\Delta$  is negligible. We also neglect the effective long-range repulsion between the composites which can further stabilize the  $CH1$  phase. Within weak-

coupling limit the mean-field parameters can be defined:

$$\begin{aligned}
\langle \hat{p}_{xBi}^\dagger \hat{p}_{yCj} \rangle &= \langle \hat{p}_{yBi}^\dagger \hat{p}_{xCj} \rangle = i\chi_{QAH}, \\
\langle \hat{p}_{xBi}^\dagger \hat{p}_{yCj} \rangle &= -\langle \hat{p}_{yBi}^\dagger \hat{p}_{xCj} \rangle = i\chi_{QSH}, \\
\langle \hat{n}_{xBi} \rangle - \langle \hat{n}_{yCj} \rangle &= \langle \hat{n}_{xCi} \rangle - \langle \hat{n}_{yBj} \rangle = \chi_{SN},
\end{aligned}
\tag{7}$$

where  $\chi_{QAH}$  denotes the order parameter for the *QAH* state that generates loop-current with broken time-reversal symmetry (TRS). Such state carries topologically protected chiral-edge states. The *QSH* order parameter  $\chi_{QSH}$  can be thought of as two systems showing *QAH* effect each breaking TRS, but on the whole both systems jointly preserve the TRS. Such states contain helical edge states as shown in [36]. On the other hand, the spin-nematic state (SN) order parameter  $\chi_{SN}$  breaks  $C_4$  symmetry between the blue and red sub-lattices and constitutes an anisotropic semi-metal [17]. We plot the resulting phase diagram in Fig.2(d) as a function of  $\alpha = a_s/a$  and dipolar strength  $D$ . In the blue region, the ground state is given by the spin-nematic phases, whereas in the green region the ground state is topologically insulating *QAH/QSH* phase. Within the mean-field ansatz (7) both *QAH* and *QSH* have the same energy, although this degeneracy can be broken by including higher order exchange interactions [16]. The corresponding mean-field transition temperature to the *QAH/QSH* state is given by,  $T_c \sim (4J_{01}^2/\Delta) \exp[-J_{01}^2/2V_{xx}\Delta] \sim 0.01E_R$  for  $D = 0.29$  and  $\alpha = -0.7$ .

### Conclusion

In conclusion, we have presented a theoretical proposal to dynamically create frustrated lattices. With this we have provided a novel way to look into emergent structures which not only create exotic dispersion relations but also induces pseudo-spin degree of freedom. We believe that our proposal opens up another fascinating route for experimental and theoretical studies of frustrated systems. For example, depending on the experimental preparation such dynamical lattices can have domain structures due to the different orientation of the *CH1* structures. This will induce in principle domain-dependent edge currents in the bulk of the sample, which can induce quantum Hall like plateaux. Also the proposed method is very general and can be extended to other lattice structures even in three dimensions. Another potential experimental advantage of our proposal is that it does not involve additional optical components other than the ones needed for creating the parent lattice.

### Acknowledgement

We acknowledge the support by the EU STREP EQUaM, IP AQUATE and SIQS, ERC Grant QUAGATUA, AAIL-Hubbard. O. D. also acknowledges support from DEC-2012/04/A/ST2/00088. A. P. is supported by the International PhD Project "Physics of future quantum-based information technologies", grant MPD/2009-3/4 from Foundation for Polish Science and by the University of Gdańsk grant BW 538-5400-0981-12. A.P. also acknowledges hospitality from ICFO.

---

\* omjyoti@gmail.com

- [1] C. Nayak, *et. al.*, Rev. Mod. Phys. **80**, 1083 (2008).
- [2] M. Lewenstein, A. Sanpera, and V. Ahufinger, Ultracold Atoms in Optical Lattices: Simulating quantum many-body systems, Oxford University Press, London, (2012).
- [3] M. Z. Hasan, and C. L. Kane, Rev. Mod. Phys. **82**, 3045 (2010).
- [4] X.-L. Qi, and S.-C. Zhang, Rev. Mod. Phys. **83**, 1057 (2011).
- [5] F. D. M. Haldane, Phys. Rev. Lett. **61**, 2015 (1988).
- [6] J. Struck, *et. al.*, Science **333**, 996 (2011).
- [7] G.-B. Jo, *et. al.*, Phys. Rev. Lett. **108**, 045305 (2012).
- [8] G. Wirth, M. Ölschläger, and A. Hemmerich, Nat. Phys. **7**, 147 (2011).
- [9] L. Tarruell, *et. al.*, Nature **483**, 302 (2012).
- [10] M. Aidelsburger, *et. al.*, Phys. Rev. Lett. **107**, 255301 (2011).
- [11] P. Hauke, *et. al.*, Phys. Rev. Lett. **109**, 145301 (2012).
- [12] T. Neupert, L. Santos, C. Chamon, and C. Mudry, Phys. Rev. Lett. **106**, 236804 (2011).
- [13] K. Sun, W. V. Liu, A. Hemmerich, and S. Das Sarma, Nat. Phys. **8**, 67 (2012).
- [14] N. Y. Yao, *et. al.* Arxiv: 1212.4839 (2012).
- [15] N. Goldman, F. Gerbier, M. Lewenstein, Arxiv: 1301.4959 (2013).
- [16] S. Raghu, X.-L. Qi, C. Honerkamp, and S.-C. Zhang, Phys. Rev. Lett. **100**, 156401 (2008).
- [17] K. Sun, H. Yao, E. Fradkin, and S. A. Kivelson, Phys. Rev. Lett. **103**, 046811 (2009).
- [18] R. Micnas, J. Ranninger, and S. Robaszkiewicz, Rev. Mod. Phys. **62**, 113 (1990).
- [19] A. Kuklov, N. Prokof'ev, and B. Svistunov, Phys. Rev. Lett. **92**, 030403 (2004).
- [20] M. Lewenstein, L. Santos, M. A. Baranov, and H. Fehrmann, Phys. Rev. Lett. **92**, 050401 (2004).
- [21] O. Dutta, *et. al.*, New J. Phys. **13**, 023019 (2011).
- [22] T. Sowiński, *et. al.*, Phys. Rev. Lett. **108**, 115301 (2012)
- [23] O. Dutta, T. Sowiński, and M. Lewenstein, arXiv: 1202.4158.
- [24] D.-S. Lühmann, O. Jürgensen, and K. Sengstock, New J. Phys. **14**, 033021 (2012).
- [25] S. Will, *et. al.*, Nature **465**, 197 (2010).
- [26] R. Lemański, J. K. Freericks, and G. Banach, Phys. Rev. Lett. **89**, 196403 (2002).
- [27] A review of such systems can be found on Chs. (6) and (8) of [2]
- [28] T. Bourdel, *et. al.*, Phys. Rev. Lett. **93**, 050401 (2004).

- [29] M. Bartenstein, *et. al.*, Phys. Rev. Lett. **92**, 120401 (2004).  
 [30] C. Kohstall, *et. al.*, Nature 485, 615 (2012).  
 [31] J. Dalibard, F. Gerbier, G. Juzeliūnas, and P. Öhberg, Rev. Mod. Phys. **83**, 1523 (2011).  
 [32] J. Struck, *et. al.*, Phys. Rev. Lett. **108**, 225304 (2012).  
 [33] S. Uebelacker, and C. Honerkamp, Phys. Rev. B **84**, 205122 (2011).  
 [34] M. Lu, N. Q. Burdick, and B. L. Lev, Phys. Rev. Lett. **108**, 215301 (2012).  
 [35] K. Aikawa, *et. al.*, Phys. Rev. Lett. **108**, 210401 (2012).  
 [36] C. Wu, B. A. Bernevig, and S.-C. Zhang, Phys. Rev. Lett. **96**, 106401 (2006).  
 [37] W. Kohn, Phys. Rev. **115**, 809 (1959).  
 [38] P. R. Johnson, E. Tiesinga, J. V. Porto, and C. J. Williams, New. J. Phys. **11**, 093022 (2009).

### Supplementary Material for *Topological insulators in dynamical lattices*

#### Derivation of $J_{01}$ and $J_{11}$ in the modified Hamiltonian

Here we describe the procedure to calculate the terms in the modified Hubbard model in Eq. (1), (2) and (3). The fermions are moving in the potential

$$V_{\sigma,\text{latt}} = V_{\sigma,x} \sin^2(\pi x/a) + V_{\sigma,y} \sin^2(\pi y/a) + V_{\sigma,z} \sin^2(\pi z/a),$$

where  $\sigma = \uparrow, \downarrow$  denotes the two species and  $V_{\sigma,x(y)(z)}$  are the corresponding lattice depths for  $\sigma$ -fermions along the  $x, y, z$  direction respectively. For the two-dimensional (2D) geometry we choose  $V_0 = V_{\downarrow,x} = V_{\downarrow,y}$ ,  $V_1 = V_{\downarrow,z} = V_{\uparrow,x(y)(z)}$ , and  $V_1 \gg V_0$ , which means that the  $\downarrow$ -fermions can effectively move in the  $x-y$  plane with the  $z$  motion frozen. The contact-interaction Hamiltonians is given by,

$$H_{\text{con}} = \frac{g}{2} \sum_{\sigma \neq \sigma'} \int \hat{\Psi}_{\sigma}^{\dagger}(\vec{r}) \hat{\Psi}_{\sigma'}^{\dagger}(\vec{r}) \hat{\Psi}_{\sigma'}(\vec{r}) \hat{\Psi}_{\sigma}(\vec{r}) d\vec{r}, \quad (8)$$

where the field operators  $\hat{\Psi}_{\sigma}^{\dagger}(\vec{r}), \hat{\Psi}_{\sigma}(\vec{r})$  denotes the creation and destruction operators at position  $\vec{r}$  for fermionic species  $\sigma$ . We also assume for simplicity that the mass of the two species are same  $m_{\uparrow} = m_{\downarrow} = m$ . The contact interaction is given by  $g = 4\pi\hbar^2 a_s/m$ . From that, we construct the Wannier functions corresponding to the band  $M = (m_x, m_y, m_z)$  is  $\mathcal{W}_{\mathbf{i},\sigma}^M(x, y, z) = \omega_{i_x,\sigma}^{m_x}(x) \omega_{i_y,\sigma}^{m_y}(y) \omega_{i_z,\sigma}^{m_z}(z)$  localized at site  $\mathbf{i} = (i_x, i_y, i_z)$  [37]. Due to strong trapping along the  $z$  direction, we only take into account the the lowest level in that direction. By expanding the field operator in the Wannier basis, we derive the parameters for the Hubbard model. In particular, the integrals used to calculate the  $s-p$  hopping term  $J_{01}$  and the correlated hopping term in  $p$ -band

$J_{11}$  are:

$$\begin{aligned} \frac{J_{01}}{E_R} &= \frac{8\pi^2 a_s}{a} \int d\mathbf{r} \mathcal{W}_{\mathbf{i},\downarrow}^{100}(\mathbf{r}) [\mathcal{W}_{\mathbf{i},\uparrow}^{000}(\mathbf{r})]^2 \mathcal{W}_{\mathbf{j},\downarrow}^{000}(\mathbf{r}), \\ \frac{J_{11}}{E_R} &= \frac{8\pi^2 a_s}{a} \int d\mathbf{r} \mathcal{W}_{\mathbf{i},\downarrow}^{100}(\mathbf{r}) [\mathcal{W}_{\mathbf{i},\uparrow}^{000}(\mathbf{r})]^2 \mathcal{W}_{\mathbf{j},\downarrow}^{100}(\mathbf{r}), \end{aligned} \quad (9)$$

where  $\mathbf{ij}$  is the nearest neighbouring sites along  $x$ -direction. As depicted in Fig.1(b) and (c) in the main paper, the effective tunneling in the  $p$ -band is given by  $J_p = J_1 + 2J_{11}$ . subsequently corresponding to Hamiltonian in Eq. (2), we plot the magnitudes of the corresponding parameters in Fig.3. We see that with increasing attraction, the effective hybridized tunneling  $J_{01}$  becomes comparable to the tunneling in the  $p$ -band, denoted by  $J_p$ . Additionally we also plot the energy cost  $\Delta$  (as defined after Eq. (2) in the main manuscript) as a function of effective interaction  $a_s/a$  in Fig.3. For small  $|a_s|/a_s$ , the energy cost  $\Delta$  is positive. As one increases the attraction,  $\Delta$  decreases and for  $a_s/a \lesssim -0.56$ ,  $\Delta$  becomes negative. Now the appearance of  $CH1$  state is favoured when the  $s-p$  tunneling strength becomes same order of magnitude as the tunneling in  $p$ -band with  $J_{01} \approx J_p = J_1 + J_{11}$  for  $\Delta \lesssim 0$ . From 3 we see that around  $|\alpha| \sim 0.5 - 0.6$  both the tunneling have the same order of magnitude facilitating the checkerboard phase.

#### Derivation of $U_3$ and $U_2$ in the modified Hamiltonian

Next we describe procedure to generate the effective interactions  $U_2$  and  $U_3$  in the modified Hamiltonian Eq.(2). As described in the paper, one of the the main parameter which controls the transition is energy cost  $\Delta = E_1 - |U_3| + |U_2|$ . Thus the main quantity to consider is the difference  $U_3 - U_2$ . To do that first we expand (8) in terms of the Wannier functions at a site  $\mathbf{i}$ ,

$$\begin{aligned} H_{\mathbf{i}} &= \sum_{MNPQ} f_{MNPQ} \hat{c}_{M,\mathbf{i}}^{\dagger} \hat{b}_{N,\mathbf{i}}^{\dagger} \hat{b}_{P,\mathbf{i}} \hat{c}_{Q,\mathbf{i}} \\ &+ \sum_M E_M^c \hat{c}_{M,\mathbf{i}}^{\dagger} \hat{c}_{M,\mathbf{i}} + \sum_M E_M^b \hat{b}_{M,\mathbf{i}}^{\dagger} \hat{b}_{M,\mathbf{i}} \end{aligned} \quad (10)$$

where  $MNPQ$  are the band indices and  $\hat{c}_{M,\mathbf{i}}^{\dagger}, \hat{c}_{M,\mathbf{i}}$  denotes the creation and annihilation operators for the  $\downarrow$ -fermions in site  $\mathbf{i}$  and band  $M$ . Similarly,  $\hat{b}_{N,\mathbf{i}}^{\dagger}, \hat{b}_{N,\mathbf{i}}$  denotes the creation and annihilation operators for the  $\uparrow$ -fermions in site  $\mathbf{i}$  and band  $N$ .  $E_M^c$  and  $E_M^b$  are the single-particle energies for the  $\downarrow$  and  $\uparrow$ -fermions respectively at the band  $M$ . The effective strengths  $f_{MNPQ}$  is given in terms of Wannier functions as,

$$\frac{f_{MNPQ}}{E_R} = \frac{8\pi^2 a_s}{a} \int d\mathbf{r} \mathcal{W}_{\mathbf{i},\downarrow}^M(\mathbf{r}) \mathcal{W}_{\mathbf{i},\uparrow}^N(\mathbf{r}) \mathcal{W}_{\mathbf{i},\uparrow}^P(\mathbf{r}) \mathcal{W}_{\mathbf{i},\downarrow}^Q(\mathbf{r}).$$

Now to determine  $U_2$ , we first assume that the particles are occupying the lowest band. Then we calculate

$$\begin{aligned}
H_2 &= -|f_{0000}| \hat{c}_{0,i}^\dagger \hat{b}_{0,i}^\dagger \hat{b}_{0,i} \hat{c}_{0,i} + \sum_M E_0^c \hat{c}_{0,i}^\dagger \hat{c}_{0,i} + \sum_M E_M^b \hat{b}_{0,i}^\dagger \hat{b}_{0,i}, \\
H_{2\text{pert}} &= \sum_{M>0} f_{M000} \hat{c}_{M,i}^\dagger \hat{b}_{0,i}^\dagger \hat{b}_{0,i} \hat{c}_{0,i} + \sum_{M>0, N>0} f_{MN00} \hat{c}_{M,i}^\dagger \hat{b}_{M,i}^\dagger \hat{b}_{0,i} \hat{c}_{0,i},
\end{aligned} \tag{11}$$

where in the diagonal term  $H_2$ , the first term is the interaction energy of the fermions in the lowest band and the next two terms denote the single-particle energies of the lowest bands for the  $c$ - and  $b$ -fermions. In the perturbative Hamiltonian  $H_{2\text{pert}}$ , the first term denotes the transition of fermion species  $c$ -( $=\downarrow$ ) to higher levels due to the interaction whereas the last term denotes the process where both  $c$ -( $=\downarrow$ ) and  $b$ -( $=\uparrow$ ) fermions are transferred to an excited state. Then for perturbation theory

the effect of the higher bands within second order perturbation theory by taking into account transitions to higher bands. Then the Hamiltonian is,

to be valid, the first condition is,

$$\begin{aligned}
& \left| \frac{f_{M000}}{(E_M^c - E_0^c) + |f_{0000}| - |f_{M00M}|} \right| \ll 1, \\
& \left| \frac{f_{MN00}}{(E_M^c - E_0^c) + (E_N^b - E_0^b) + |f_{0000}| - |f_{MN00}|} \right| \ll 1
\end{aligned} \tag{12}$$

To look into their properties, first we note that  $|f_{MN00}|, |f_{M00M}|, |f_{M000}|, |f_{MN00}| < |f_{0000}|$  as interaction in the lowest band has the strongest value. In addition,  $(E_M^c - E_0^c) > 0, (E_N^b - E_0^b) > 0$  for band indices  $M, N > 0$ . So the denominators are always positive and we numerically checked that the fractions are much less than unity. This situation is drastically different for repulsive interactions where the denominator can indeed vanish making the perturbation theory invalid. Then within second-order perturbation theory we can write the two-fermion interaction energy,

$$U_2 = -|f_{0000}| - \sum_{M>0} \frac{f_{M000}^2}{(E_M^a - E_0^a) + |f_{0000}| - |f_{M00M}|} - \sum_{MN>0} \frac{f_{MN00}^2}{(E_M^a - E_0^a) + (E_N^b - E_0^b) + |f_{0000}| - |f_{MN00}|} \tag{13}$$

Similarly one can write the Hamiltonian pertaining to the situation when there are two  $\downarrow$  ( $c$ -) particles, one as the  $s$ -band and another at the  $p_x$ -band, and one  $\uparrow$  ( $b$ -) fermion in the  $s$ -band. The corresponding interaction energy  $U_3$  is written in second-order perturbation as,

$$\begin{aligned}
U_3 &= -|f_{0000}| - |f_{1001}| - \sum_{M \neq [0,1]} \frac{f_{M000}^2}{(E_M^c - E_0^c) + |f_{0000}| - |f_{M00M}|} - \sum_{M \neq [0,1]} \frac{f_{M001}^2}{(E_M^c - E_1^c) + |f_{1001}| - |f_{M00M}|} \\
&\quad - \sum_{M \neq [0,1], N > 0} \frac{f_{MN00}^2}{(E_M^c - E_0^c) + (E_N^b - E_0^b) + |f_{0000}| + |f_{1001}| - |f_{1MM1}| - |f_{MN00}|} \\
&\quad - \sum_{M \neq [0,1], N > 0} \frac{f_{MN01}^2}{(E_M^c - E_1^c) + (E_N^b - E_0^b) + |f_{0000}| + |f_{1001}| - |f_{0MM0}| - |f_{MN01}|},
\end{aligned} \tag{14}$$

where the band index  $1 = (100)$  denotes the  $p_x$ -band. The individual series in Eqs.(13), (14) does not converge

with respect to the summation over band indices  $M, N$  and one need to regularize the interaction at higher ener-

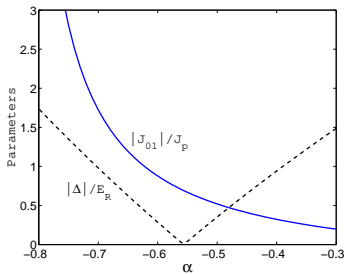


FIG. 3. In this figure we plot the important parameters in our paper, namely, the energy cost  $|\Delta|/E_R$  (black dashed line) and the relative strength of the  $s - p$ -band tunneling and the effective tunneling in  $p$ -band,  $J_{01}/|J_p|$  (the blue solid line), as a function of the effective interaction strength  $\alpha = a_s/a$ . We fix the  $\downarrow$ -fermion lattice depth  $V_0 = 4E_R$  and the  $\uparrow$ -fermion lattice depth  $V_1 = 30E_R$  for which we see from Fig.(2) in the paper that the *CHI* state is stable. For low  $\alpha$ ,  $\Delta$  is positive. As  $\alpha$  becomes more negative,  $\Delta$  decreases. For  $\alpha \lesssim -0.56$ ,  $\Delta$  becomes negative and its absolute value increases. From the blue curve we also see that with increase in  $|\alpha|$ , the effective  $p$ -band tunneling decreases and  $s - p$  tunneling increases resulting in an increase in the ratio  $J_{01}/J_p$ . Around  $\alpha \sim -0.6$  contribution of each tunneling processes become of the same order of magnitude facilitating the stability of the *CHI* phase in the paper.

gies. But in this paper we are only interested in the difference in energy  $U_3 - U_2$  which converges as one takes bands with higher energies. In our parameter regime  $U_3 - U_2$  converges for band indices  $M = 15$ . Convergence of the differences between the energies are also discussed in Ref.[38] using the harmonic approximation for the lattice sites.